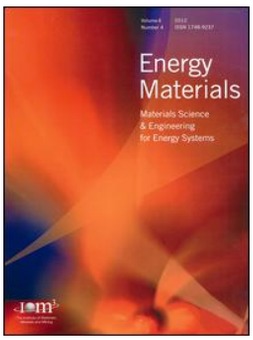

Energy Materials

Advanced Performance Materials

ISSN: 1066-7857 (Print) 1753-5557 (Online) Journal homepage: http://www.tandfonline.com/loi/yema20

TiO_2 nanowire arrays with mixed phases directly grown on Ti foil and their electrochemical properties as anode material for Li ion batteries

W Xiong, Y D Wang & H Xia

To cite this article: W Xiong, Y D Wang & H Xia (2013) TiO_2 nanowire arrays with mixed phases directly grown on Ti foil and their electrochemical properties as anode material for Li ion batteries, Energy Materials, 28:5, 260-264

To link to this article: http://dx.doi.org/10.1179/1753555713Y.0000000069@yema20.2013.8.issue-4

Published online: 18 Nov 2013.

TiO_2 nanowire arrays with mixed phases directly grown on Ti foil and their electrochemical properties as anode material for Li ion batteries

W. Xiong[1], Y. D. Wang*[2] and H. Xia*[1]

TiO_2 nanowire arrays with mixed phases are directly grown on Ti foil using a facile hydrothermal method. X-ray diffraction and Raman spectroscopy analyses indicate that the hybrid samples consist of mixed crystallographic phases of anatase and TiO_2(B). Morphological characterisation shows that the samples have a unique nanostructure with ultra long, fine and uniform nanowires. Compared with the standard Degussa P25 TiO_2 nanoparticles, the hybrid TiO_2 nanowire arrays exhibit larger reversible capacity, improved cycling stability and rate capability, which can be attributed to their hybrid nanowire array structure.

Keywords: Nanowire arrays, TiO_2(B), Anatase, Lithium ion batteries, Hybrid

This paper is part of a special issue on Functional Materials for Device and Energy Applications

Introduction

Lithium ion batteries have been the dominant power source for a myriad of types of portable electronic devices[1] and potential power source for electric vehicles[2] because of their advantages such as no memory effect, high energy density, long life cycle and low toxicity in comparison with the other rechargeable batteries.[3–5] Given that the performance of lithium ion batteries strongly depends on the electrode properties, fundamental improvements are needed with regard to power, safety, cycle life, cost, etc. Most of commercial lithium ion batteries use graphite as the anode. However, the graphite electrode has several disadvantages including its electrical disconnection, structural deformation and initial loss of capacity.[6–10] The intrinsic safety problem caused by the organic electrolyte decomposition is attributed to the low discharge potential of graphite anode. TiO_2 has been considered as a good alternative to graphite due to its suitable discharge potential (about 1·5–1·7 V(Li/Li^+)), which would not induce the decomposition of organic electrolyte.[11] Along with the advantages in terms of abundance, low cost and environmental benignity, TiO_2 has attracted a lot of interest as anode material for lithium ion batteries. The electrochemical properties of TiO_2 electrodes can be significantly improved by optimising the size, morphology or porosity of the structure.[12–14] Recently, nanostructured TiO_2 as the anode materials for lithium ion batteries stimulated extensive research since they demonstrated excellent improvement in electrochemical performance compared to the respective micrometre material.[15–20]

TiO_2 exists in different polymorphic forms, such as rutile, anatase, bronze or TiO_2(B). One-dimensional anatase TiO_2 nanotubes or nanowires are usually considered as one of the most promising anode materials for lithium ion batteries. However, their low lithium ion diffusivity and poor electronic conductivity limit the practical application.[21,22] It has been demonstrated that the introduction of TiO_2(B) into the anatase TiO_2 can enhance the electronic conductivity and lithium ion diffusivity due to the one-way valve heterojunction at their interfaces and the continuous channel-like structure of TiO_2(B).[23,24] As for electrode fabrication, designing nanowire arrays growing directly on a current collector represent a novel approach, reducing the extra weight of binders or conducting additives for making battery electrodes.

In this work, TiO_2 nanowire arrays with mixed phases of anatase and TiO_2(B) were grown on Ti foil by a simple hydrothermal treatment of Ti foil in alkaline medium, followed by proton exchange and thermal annealing. The structural characterisation revealed that anatase and TiO_2(B) coexist in the nanowire arrays. Compared with standard Degussa P25 TiO_2 nanoparticles, the TiO_2 nanowire arrays with mixed phases exhibited superior electrochemical properties attributing to their hybrid nanowire array structure.

Experimental

The hybrid TiO_2 nanowire arrays were synthesised by a simple hydrothermal method with similar procedure reported by Wang *et al.*[25] High purity Ti foils (99·95%,

[1]School of Materials Science and Engineering, Nanjing University of Science and Technology, Nanjing 210094, China
[2]School of Engineering, Nanyang Polytechnic, 180 Ang Mo Kio Ave 8, Singapore 569830, Singapore

*Corresponding authors, email smap1018@gmail.com; xiahui@njust.edu.cn

Received 4 December 2012; accepted 7 February 2013
DOI 10.1179/1753555713Y.0000000069

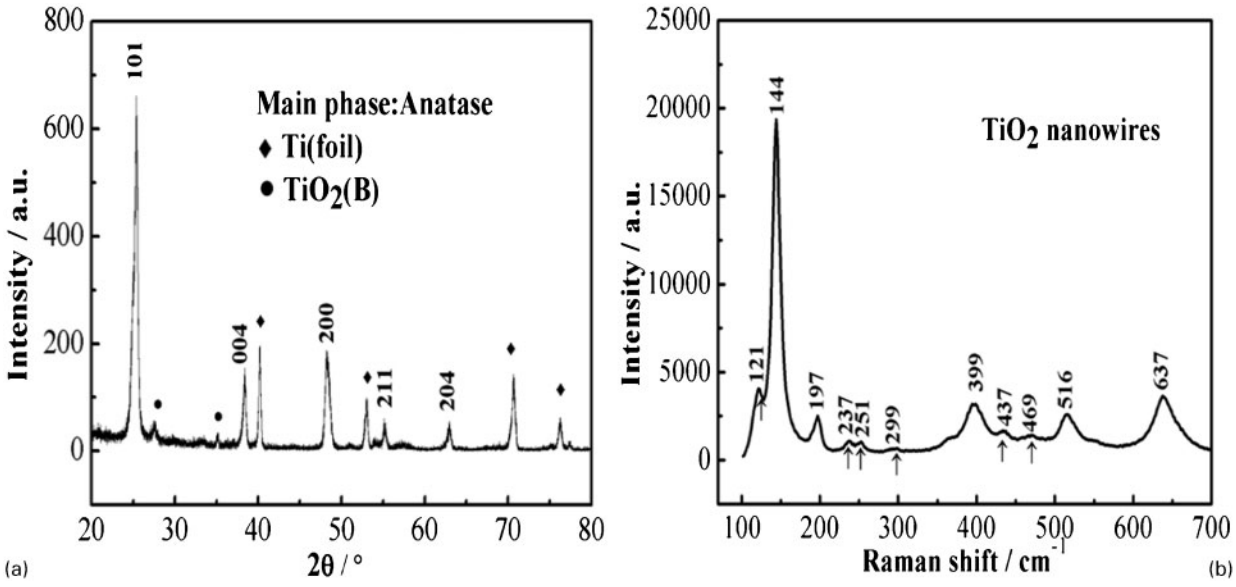

1 ***a*** **XRD pattern of hybrid TiO_2 nanowire arrays and** ***b*** **Raman spectrum of hybrid TiO_2 nanowire arrays**

Goodfellow) were sanded first with 250 grit and then with 600 grit SiC paper, then cleaned by sonication in ethanol, acetone and deionised water respectively, and finally dried in a nitrogen gas flow. The dried Ti foil was put into a 125 mL Teflon lined stainless steel autoclave filled with 60 mL 1M NaOH solution. The autoclave was put in an electric oven at 220°C for 20 h and then air cooled to room temperature. The produced samples were washed with deionised water and immersed into 0·6M hydrochloric acid for 24 h. Finally, the as washed samples were calcined at 600°C for 2 h.

The structure and crystallinity of the as prepared samples were characterised by X-ray diffraction (XRD) and Raman spectroscopy. X-ray diffraction patterns of the samples were recorded on a Shimadzu XRD-6000 X-ray diffractometer with Cu K_α radiation. Data were collected in the 2θ range of 20–80° at a scan rate of 2° min^{-1}. Raman spectra were recorded on a Jobin-Yvon HR800 instrument with an Ar^+ laser source of 488 nm wavelength in a macroscopic configuration. Surface morphology of the samples was characterised using a Hitachi S-4100 field emission scanning electron microscope (FESEM) and a transmission electron microscope (TEM, JEOL, JEM-2010).

The electrochemical measurements were carried out on Swagelok type cells using LANDCT2001A battery system. For comparison, the standard P25 TiO_2 was chosen for battery performance test. The P25 TiO_2 working electrode was prepared by coating a slurry, composed of 80 wt-%P25 TiO_2, 10 wt-% polyvinylidene difluoride binder and 10 wt-% conducting carbon black additive in *N*-methyl-2-pyrrolidinone, on a Ti foil and dried in a vacuum oven for 12 h. The TiO_2 nanowire arrays grown on Ti foil were directly used as the working electrode without any binders or conducting additives. To evaluate the mass of TiO_2 nanowire arrays, TiO_2 nanowire arrays were carefully stripped from the Ti substrate using a doctor blade. The net mass of the TiO_2 nanowire arrays was measured by weighing the Ti substrate before and after stripping the TiO_2 nanowire arrays using a microelectronic balance with precision of 1 μg. $LiPF_6$ (1M) in ethylene carbonate and diethyl carbonate (EC/DEC=1 : 1, v/v) solution was used as the electrolyte, and lithium foil was used as both the counter and the reference electrodes. Galvanostatic charge and discharge measurements were carried out in the voltage range from 1·0 to 3·0 V at different current densities from 100 to 1600 mA g^{-1}. Cyclic voltammograms (CVs) and electrochemical impedance spectroscopy (EIS) were performed using a CHI660D electrochemical workstation. Cyclic voltammograms were recorded between 3·0 and 1·0 V at a scan rate of 0·1 mV s^{-1}. Spectra by EIS were carried out with an ac amplitude of 10 mV over the frequency range from 100 kHz to 0·01 Hz.

Results and discussion

The XRD spectrum and Raman spectrum of the hybrid TiO_2 nanowire arrays are shown in Fig. 1. As shown in Fig. 1*a*, except for the diffraction peaks from Ti foils, all other diffraction peaks can be indexed based on the anatase (JCPDS no. 83-2243) and TiO_2(B) (JCPDS no. 74-1940). Diffraction peaks corresponding to the TiO_2(B) phase are not very distinguishable, which is probably due to the small grain size and the overlapping with those of the anatase phase. The structure of the hybrid TiO_2 nanowire arrays was further investigated by Raman spectroscopy, which is more sensitive to the microstructure of materials than XRD. Figure 1*b* shows the Raman spectrum of the hybrid TiO_2 nanowire arrays. The Raman modes at 144 cm^{-1} (E_g), 197 cm^{-1} (E_g), 399 cm^{-1} (B_{1g}), 513 cm^{-1} ($A_{1g}+B_{1g}$) and 628 cm^{-1} (E_g) respectively are in well agreement with the typical Raman features of the anatase phase.[24] In addition, another six Raman modes with weaker intensity marked by arrows are attributed to the TiO_2(B) phase.[24,25] Agreeing well with the XRD results, the Raman results confirm the hybrid structure of the TiO_2 nanowire arrays composed of anatase and TiO_2(B).

The morphologies of the standard P25 TiO_2 sample and the hybrid TiO_2 nanowire arrays were characterised by FESEM as shown in Fig. 2. Figure 2*a* shows the FESEM image of the P25 TiO_2, in which the nanoparticles with a particle size between 30 and 60 nm are closely aggregated. Figure 2*b* and *c* shows the FESEM images of the hybrid TiO_2 nanowire arrays at low and

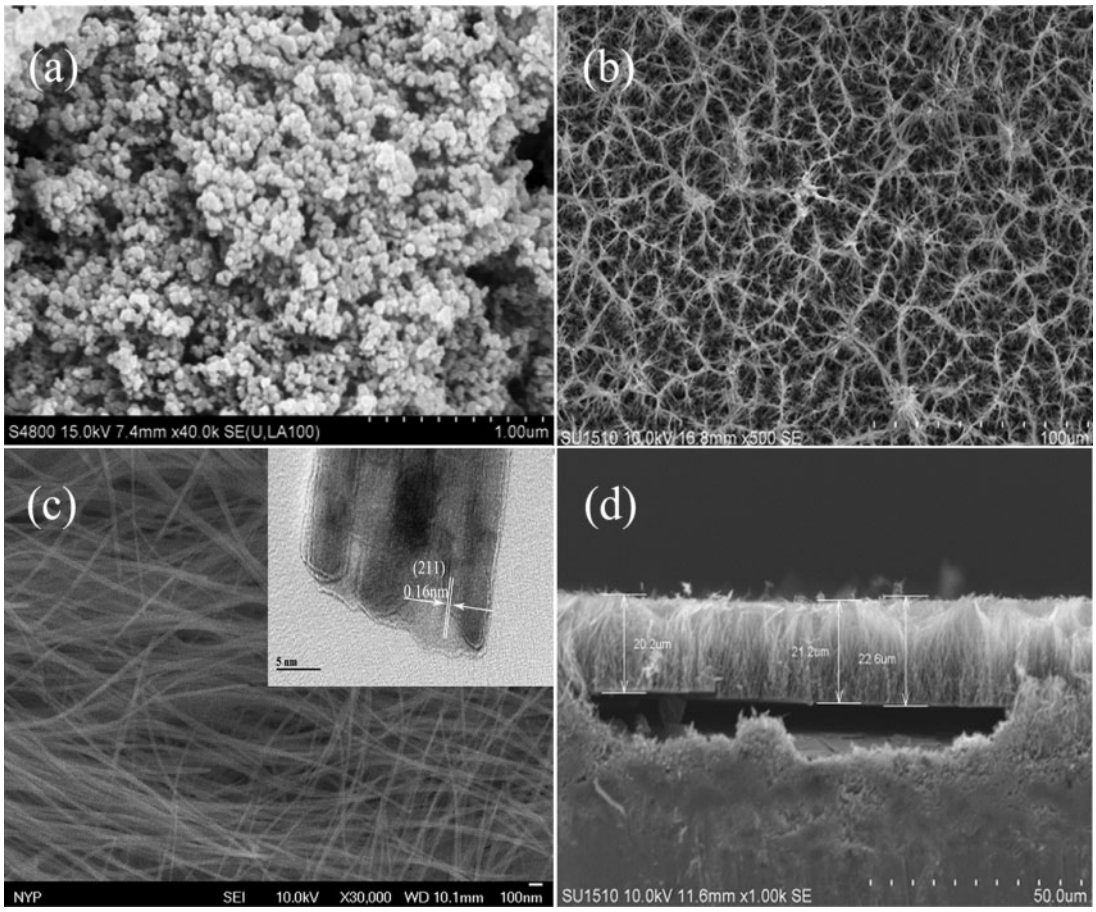

2 *a* FESEM image of P25 TiO_2 nanoparticles, *b*, *c* FESEM images of hybrid TiO_2 nanowire arrays and *d* cross-section FESEM image of hybrid TiO_2 nanowire arrays (inset in *c* gives high resolution TEM of single TiO_2 nanowire)

high magnifications. It can be seen that the film displays a highly porous network morphology. The magnified image shows that the network consists of ultrafine TiO_2 nanowires with an average diameter of $\sim$20 nm. Since the diameters of the titanate nanowires are very small, they tend to bend or enlace with other nanowires as their length increases. Therefore, the TiO_2 nanowire arrays looks like a porous network structure from the top view. Inset in Fig. 2*c* gives the high resolution TEM image of a single TiO_2 nanowire. The lattice fringe with interplanar spacing of 0·16 nm can be attributed to (211) planes of anatase TiO_2. The cross-section FESEM image (Fig. 2*d*) shows that the orientated nanowires are perpendicularly grown on the Ti foil, and the thickness is $\sim$21 μm.

Cyclic voltammograms of the hybrid TiO_2 nanowire array and the P25 TiO_2 electrodes for the first cycle at a scan rate of 0·1 mV s^{-1} in the voltage range of 1·0–3·0 V are shown in Fig. 3. As shown in Fig. 3*b*, CV of the P25 TiO_2 electrode exhibits one pair of redox peaks at 1·6 and 2·1 V, which is attributed to lithium insertion/extraction with respect to the anatase phase.[15] As shown in Fig. 3*a*, CV of the hybrid TiO_2 nanowire array electrode exhibits three pairs of redox peaks, with three peaks at 1·6 (S1), 1·7 (S2) and 2·1 V (A) on charge and three peaks at 1·4 (S1′), 1·5 (S2′) and 1·7 (A′) on discharge. The two pairs of redox peaks at low voltage correspond to lithium insertion/extraction with respect to the TiO_2(B) phase, agreeing well with the literature reports.[18] The pair of redox peaks at high voltage can be attributed to the anatase phase, which agrees well with redox peaks of the P25 TiO_2 electrode. The integrated area for the low voltage peaks corresponding to the TiO_2(B) is similar to that of the high voltage peaks corresponding to anatase. Considering the higher electrochemical activity of TiO_2(B), it is speculated that the molar ratio of anatase to TiO_2(B) is close to 1 but larger than 1.

Figure 4*a* and *b* shows the charge/discharge curves of the hybrid TiO_2 nanowire array electrode and the P25 TiO_2 electrode at the first, second, tenth and fiftieth cycles at a current density of 100 mA g^{-1}. The initial discharge and charge capacities of the TiO_2 nanowire array electrode are $\sim$250 and 195 mA g^{-1} respectively, which are much larger than those of the P25 TiO_2 electrode ($\sim$203 and 148 mA g^{-1}). It was reported that the precisely oriented nature of the nanostructures makes them better electron percolation pathways than the random nanoparticle systems for vectorial charge transfer between interfaces compared.[26] The greatly increased capacity can be attributed to the shorter transport lengths for both electronic and Li ion transport in the nanowire array. Severe aggregation of nanoparticles was observed in the P25 TiO_2 sample, which could block the electrolyte penetration into the centre of the aggregates, thus leading to limited contact area between electrode material and electrolyte. The hybrid TiO_2 nanowire arrays, on the other way, have a highly porous structure, providing large electrode–electrolyte contact area for lithium insertion/extraction. The hybrid TiO_2 nanowire array electrode also exhibits superior cycling stability compared to that of the P25 TiO_2 electrode.

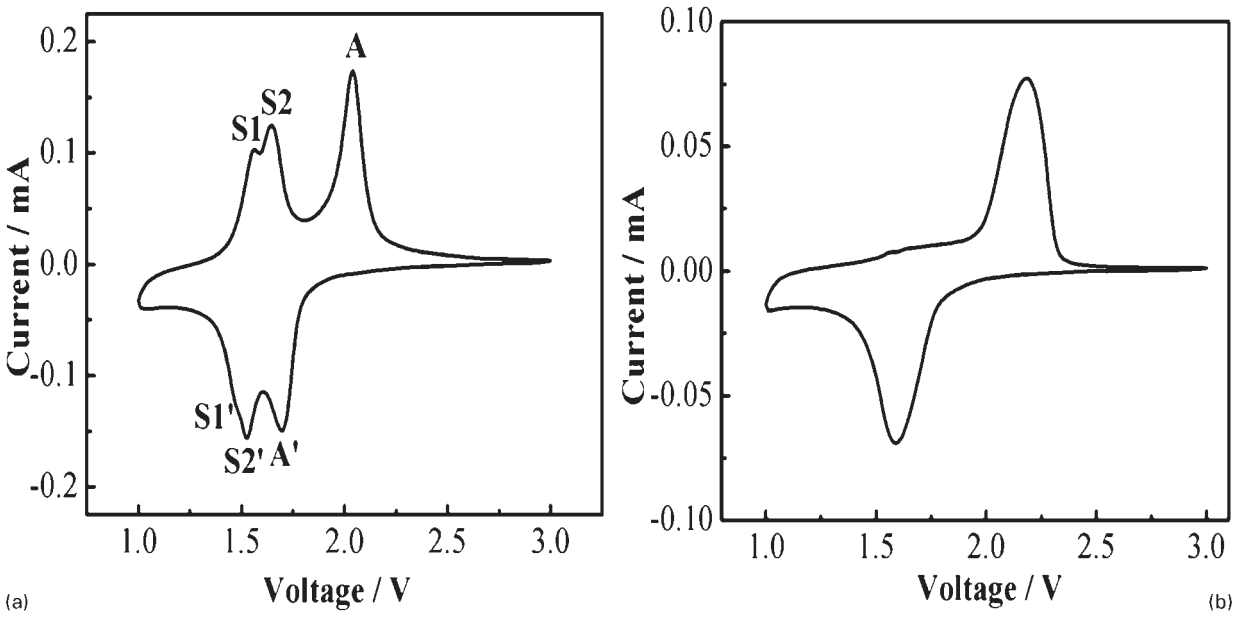

3 Cyclic voltammograms of *a* hybrid TiO_2 nanowire array electrode and *b* P25 TiO_2 electrode

After 50 cycles, the hybrid TiO_2 nanowire array electrode retains 80% of its initial reversible capacity, while P25 TiO_2 electrode only retains 60% of its initial reversible capacity. The major capacity fading of the hybrid TiO_2 nanowire arrays can be attributed to the anatase phase since the 1·75 V plateau continues decreasing with cycling. The superior cycling stability of the hybrid TiO_2 nanowire array electrode could be

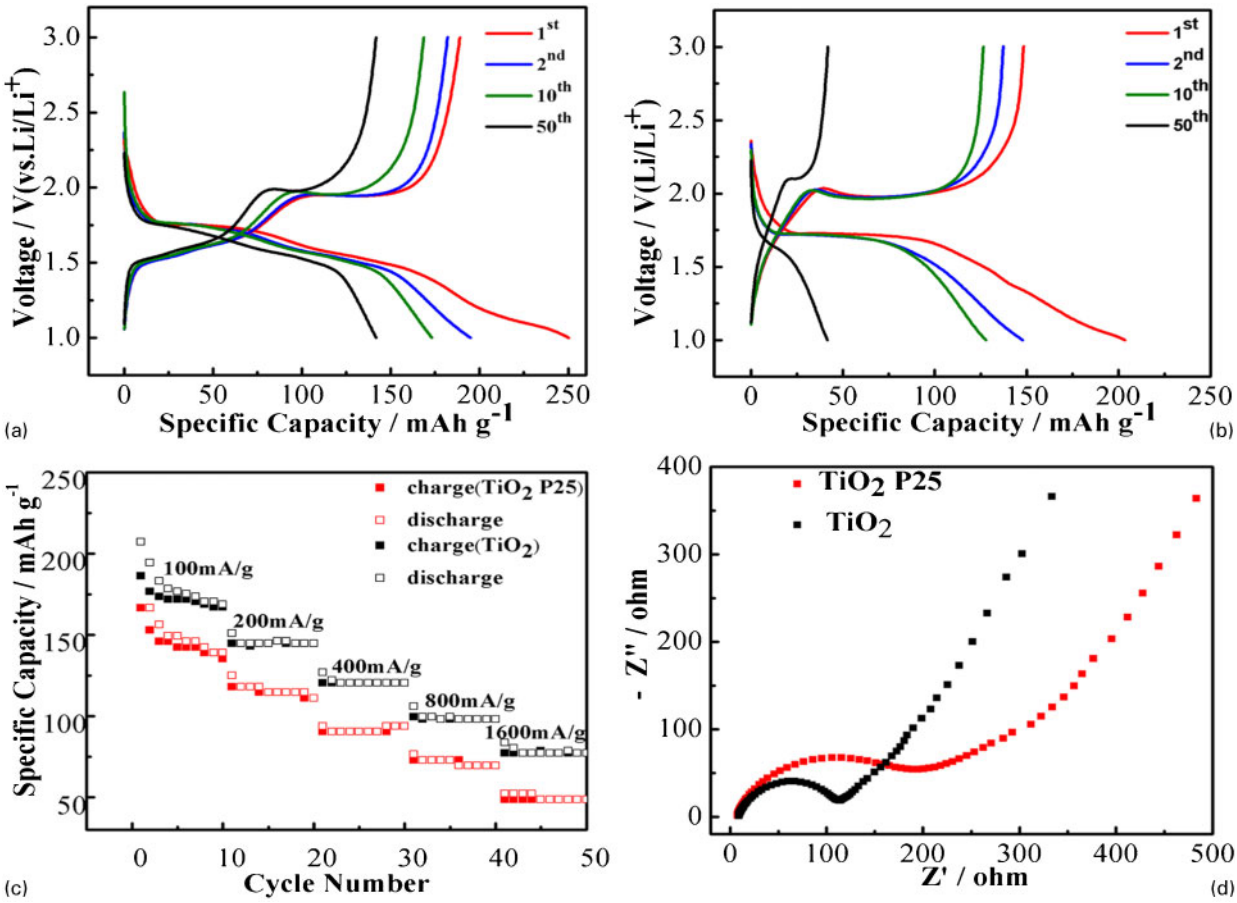

4 Charge/discharge curves for *a* hybrid TiO_2 nanowire array electrode and *b* P25 TiO_2 electrode at first, second, tenth and fiftieth cycles at current density of 100 Ma g^{-1}; *c* charge/discharge capacities of hybrid TiO_2 nanowire array electrode and P25 TiO_2 electrode as function of cycle number at various current densities and *d* Nyquist plots of hybrid TiO_2 nanowire array electrode and P25 TiO_2 electrode

attributed to its porous network structure, which has good accommodation to volume/strain changes during lithium insertion/extraction.

In addition to large reversible capacity and good cycling stability, the hybrid TiO_2 nanowire array electrode also exhibits excellent rate capability. Figure 4*c* shows charge/discharge capacities of the hybrid TiO_2 nanowire array electrode and the P25 TiO_2 electrode as a function of cycle number at a variety of current densities from 100 to 1600 mA g^{-1}. The hybrid TiO_2 nanowire array electrode delivers a reversible capacity of $\sim$166 mA h g^{-1} at 100 mA g^{-1} after 10 cycles. This value decreases to 144 mA h g^{-1} at 200 mA g^{-1}, 121 mA h g^{-1} at 400 mA g^{-1}, 98 mA h g^{-1} at 800 mA g^{-1} and 77 mA h g^{-1} at 1600 mA g^{-1}. At the same current density, the hybrid TiO_2 nanowire array electrode can deliver a much larger reversible capacity compared to the P25 TiO_2 electrode. The method of EIS was used to gain more insight into the remarkable rate capability of the hybrid TiO_2 nanowire array electrode. As shown in Fig. 4*d*, both Nyquist plots of the hybrid TiO_2 nanowire array electrode and the P25 TiO_2 electrode show a semicircle at the high frequency region, corresponding to the charge transfer resistance, and a straight line at the low frequency region, representing the diffusion resistance.[27] The hybrid TiO_2 nanowire array electrode exhibits a much smaller semicircle, indicating much smaller charge transfer resistance, which is associated with the larger surface area of the porous network. The improved charge transport capability of the hybrid TiO_2 nanowire array electrode may also be contributed by the proposed high conductivity column layer or belt formed around the heterojunction interface between anatase and TiO_2(B).[18] In particular, the polymorph of TiO_2(B) shows a favourable channel structure for lithium ion diffusion, which could result in fast charge–discharge capability. It has been identified that the lithium intercalation in TiO_2(B) features a pseudocapacitive process, rather than the solid state diffusion process observed for anatase and rutile. Furthermore, the nanowire structure could provide a direct path for excited electrons and suppress the carrier scattering between nanoparticles, which is a common phenomenon for P25 TiO_2.[24]

Conclusions

In summary, a facile hydrothermal route was employed to fabricate one-dimensional hybrid TiO_2 nanowire arrays consisting of anatase and TiO_2(B) phases. The perpendicularly grown hybrid TiO_2 nanowires with an average diameter of $\sim$20 nm and an average length of $\sim$21 μm form a highly porous network. This nanostructure provides good electrical contact between active material and current collector without using binders and conductive additives. The hybrid TiO_2 nanowire array electrode exhibits a larger reversible capacity, improved cycling stability and rate capability compared to the P25 TiO_2 electrode. The superior electrochemical performance of the hybrid TiO_2 nanowire array electrode can be attributed to its unique nanostructure and hybrid composition, which provide large electrode–electrolyte contact area, good accommodation for strain and fast charge transport.

Acknowledgements

This work was supported by National Natural Science Foundation of China (grant no. 51102134) and Nanjing University of Science and Technology through the research grant NUST Research Funding (grant nos. 2011ZDJH21 and AB41385).

References

1. J. S. Chen, L. A. Archer and X. W. J. Lou: *Chem. Mater.*, 2011, **21**, 9912.
2. V. Etacheri, R. Marom, R, Elazari, G. Salitra and D. Aurbach: *Energy Environ. Sci.*, 2011, **4**, 3243.
3. M. R. Palacin: *Chem. Soc. Rev.*, 2009, **38**, 9.
4. F. Cheng, Z. Tao, J. Liang and J. Chen: *Chem. Mater.*, 2008, **20**, 3.
5. X. P. Gao and H. X. Yang: *Energy Environ. Sci.*, 2010, **3**, 174.
6. G. Armstrong, A. R. Armstrong, P. G. Bruce, P. Reale and B. Scrosati: *Adv. Mater.*, 2006, **18**, 2597.
7. J. Xu, C. Jia, B. Cao and W. F. Zhang: *Electrochim. Acta*, 2007, **52**, 8044.
8. S. Bao, Q. Bao, C. Li and Z. Dong: *Electrochem. Commun.*, 2007, **9**, 1233.
9. S. Yoon, B. H. Ka, C. Lee, M. Park and S. M. Ohb: *Electrochem. Solid-State Lett.*, 2009, **12**, **A**28.
10. H. Qiao, Y. Wang, L. Xiao and L. Zhang: *Electrochem. Commun.*, 2008, **10**, 1280.
11. D. W. Murphy, R. J. Cava, S. M. Zahurak and A. Santoro: *Solid State Ionics*, 1983, **9**, 413.
12. G. F. Ortiz, I. Hanzu, T. Djenizian, P. Lavel, J. L. Tirado and P. Knauth: *Chem. Mater.*, 2009, **21**, 63.
13. G. Sudant, E. Baudrin, D. Larcher and J. M. Tarascon: *J. Mater. Chem.*, 2005, **15**, 1263.
14. M. Yin, Y. Cheng, M. Liu, J. Gutmann and K. Müllen: *Angew. Chem. Int. Ed.*, 2008, **47**, 8400.
15. P. F. Xiao, M. O. Lai and L. Lu: *Electrochim. Acta*, 2012, **76**, 185.
16. A. Islam, S. P. Singh and L. Y. Han: *Funct. Mater. Lett.*, 2011, **4**, 1.
17. N. F. Zhuang, R. F. Wang, X. L. Hu, C. G. Song, B. Zhao and J. Z. Chen: *Funct. Mater. Lett.*, 2011, **4**, 3.
18. Y. M. Li, X. J. Lv and J. H. Li: *Appl. Phys. Lett.*, 2009, **95**, 113102.
19. K. F. Huo, X. M. Zhang, J. J. Fu, G. X. Qian, Y. C. Xin, B. Q. Zhu, H. W. Ni and P. K. Chu: *J. Nanosci. Nanotechnol.*, 2009, **9**, 3341.
20. J. Y. Liao, B. X. Lei, H. Y. Chen and D. B. Kuang and C. Y. Su: *Energy Environ. Sci.*, 2012, **5**, 5750.
21. S. B. Yang, X. L. Feng and K. Mullen: *Adv. Mater.*, 2011, **23**, 3575.
22. S. M. Dong, H. B. Wang, G. Lin, X. H. Zho, Z. H. Liu, P. X. Han, Y. Wang, X. Chen, G. L. Cui and L. Q. Chen: *Thin Solid Films*, 2011, **519**, 5978.
23. Z. X. Yang, G. D. Du, Z. P. Guo, X. B. Yu, Z. X. Chen, T. L. Guo, N. Sharma and H. K. Liu: *Electrochem. Commun.*, 2011, **13**, 46.
24. J. X. Qiu, P. Zhang, M. Ling, S. Li, P. Liu, H. J. Zhao and S. Q. Zhang: *ACS Appl. Mater. Interfaces*, 2012, **4**, 3636.
25. C. H. Wang, X. T. Zhang, Y. L. Zhang, Y. Jia, J. K. Yang, P. P. Sun and Y. C. Liu: *J. Phys. Chem. C*, 2011, **115C**, 22276.
26. H. S. Liu, Z. H. Bi, X. G. Sun, R. R. Unocic, M. Parans Paranhaman, S. Dai and G. M. Brown: *Adv. Mater.*, 2011, **23**, 3450.
27. P. R. Bueno and E. R. Leite: *J. Phys. Chem. B*, 2003, **107B**, 8868.